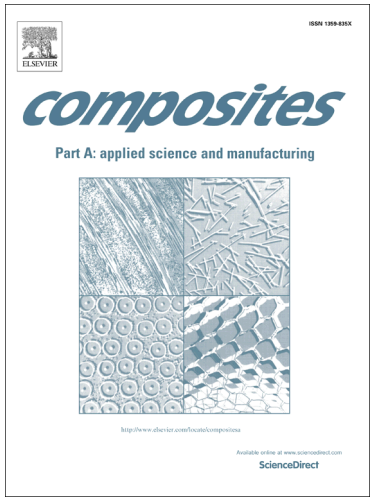

Positive size and scale effects of all-cellulose composite laminates

Jan W. Dormanns, Felix Weiler, Jeremias Schuermann, Jörg Müssig, Benoı ^t J.C. Duchemin, Mark P. Staiger

PII: S1359-835X(16)30015-X
DOI: http://dx.doi.org/10.1016/j.compositesa.2016.03.010
Reference: JCOMA 4239

To appear in: *Composites: Part A*

Received Date: 9 December 2015
Revised Date: 13 February 2016
Accepted Date: 13 March 2016

Please cite this article as: Dormanns, J.W., Weiler, F., Schuermann, J., Müssig, J., Duchemin, B.J.C., Staiger, M.P., Positive size and scale effects of all-cellulose composite laminates, *Composites: Part A* (2016), doi: http://dx.doi.org/10.1016/j.compositesa.2016.03.010

Positive size and scale effects of all-cellulose composite laminates

Jan W. Dormanns[a,b], Felix Weiler[c], Jeremias Schuermann[a,b], Jörg Müssig[c], Benoît J.C. Duchemin[d], Mark P. Staiger[a,b,*]

[a]*Department of Mechanical Engineering, University of Canterbury, Private Bag 4800, 8140 Christchurch, New Zealand*
[b] *The MacDiarmid Institute for Advanced Materials and Nanotechnology, PO Box 600, Kelburn, Wellington 6140, New Zealand*
[c]*The Biological Materials Group, Department of Biomimetics, HSB - University of Applied Sciences, Neustadtswall 30, 28199 Bremen, Germany*
[d]*Laboratoire Ondes et Milieux Complexes, UMR 6294, CNRS-Université du Havre, Le Havre, France*

Abstract

Negative size effects are commonly reported for advanced composite materials where the strength of the material decreases with increasing volume of the test specimen. In this work, the effect of increasing specimen volume on the mechanical properties of all-cellulose composites is examined by varying the laminate thickness. A positive size effect is observed in all-cellulose composite laminates as demonstrated by a 32.8 % increase in tensile strength as the laminate thickness is increased by 7 times. The damage evolution in all-cellulose composite laminates was examined as a function of the tensile strain. Enhanced damage tolerance concomitant with increasing specimen volume is associated with damage accumulation due to transverse cracking and strain delocalisation. A transition from low-strain failure to tough and high-strain failure is observed as the laminate thickness is increased. Simultaneously, scale effects lead to an increase in the void content and cellulose crystallinity at the core, with increasing laminate thickness.

Keywords: A: Laminates, A: Polymer-matrix composites (PMCs), B: Mechanical properties, Single-polymer composites (SPCs)

1. Introduction

The use of natural fibres as reinforcement in bio-based composites has received much attention due to the availability, mechanical properties and biodegradability of cellulose [1–3]. An interesting subclass of bio-based composites are all-cellulose composites (ACCs) which are single-polymer composites where both the matrix and reinforcement are based on non-derivatized cellulose [4]. Single-polymer composites are purported to have improved interfacial compatibility between the

*Corresponding author, mark.staiger@canterbury.ac.nz, tel.: +64 3 364 2987 ext. 7250

reinforcement and matrix phases compared with conventional biobased-composites that utilise hydrophilic natural fibres to reinforce a hydrophobic polymer matrix [3, 5, 6]. Hence, the mechanical properties of ACCs are found to exceed most conventional biobased-composites [7] while remaining fully bio-based and biodegradable [8].

ACCs can be processed *via* one of two routes: (i) A cellulose reinforcement (fibres or particles) is mixed with a pre-dissolved cellulose solution that forms the matrix [4]; or (ii) cellulose is brought into contact with a solvent so as to partially dissolve the surface, thereby creating a cellulose matrix *in situ* [9]. Most studies of ACCs are based on the processing and characterisation of thin films (< 1 mm). More recently, the authors have reported on the manufacture of thicker laminates (2 to 4 mm) by compression moulding [10] and solvent infusion processing (SIP) [11], with the aim of increasing the range of possible industrial applications. The ability to manufacture laminates should also allow greater customisation of the mechanical properties of ACCs, as permitted in conventional multi-axial composite laminates. In SIP, vacuum pressure is used to infuse a cellulosic textile with a solvent, similar to conventional resin infusion processes. Partial dissolution of the cellulose fibres is then triggered by a change in the temperature of the solvent. A matrix phase of regenerated cellulose is then formed *in situ* upon removal of the solvent. Subsequent drying removes the anti-solvent and results in dimensionally stable laminates with a relatively high volume fraction of fibres (> 90 %) [11]. Hence, the thickness of an ACC laminate may be controlled by simply varying the number of textile layers in the laminate stack.

The term *size effect* in composite materials, and indeed other families of materials, refers to changes in the mechanical properties caused by changes in the volume of the test specimen. In general, composite materials exhibit a negative size effect such that strength decreases with increasing specimen dimensions, as described by the weakest link theory [12–15]. The weakest link model is based on the assumption that the probability of a critical-sized, failure-inducing defect being present in a sample increases as the volume of the test specimen is increased [14, 15]. The phenomenon of size effects in composite materials has been reviewed elsewhere [12–15].

As mentioned, SIP facilitates the fabrication of ACC laminates of varying thickness. However, the effect of upscaling the specimen dimensions on the mechanical and physical properties of ACC laminates is unknown. In the present study the manifestation of size and scale effects in ACC laminates is investigated by characterising ACCs of increasing laminate thickness by tensile testing, wide-angle X-ray diffraction (WAXD) and scanning electron microscopy (SEM). Furthermore,

the evolution of damage with increasing strain is examined in a series of interrupted tensile tests followed by microstructural characterisation using SEM.

2. Experimental procedures

2.1. Materials

A regenerated cellulose fibre (Cordenka® 700, 1840 dtex, f 1000, Cordenka GmbH & Co. KG, Obernburg, Germany) in the form of a simple 2D textile (2/2 twill weave) was used as precursor for fabricating single- and multi-layered ACC laminates. The areal mass of the textile was 450 g mm^{-2}, while the yarn density was 13 and 10 yarns cm^{-1} in warp and weft direction, respectively. An ionic liquid (IL), 1-butyl-3-methylimidazolium acetate (BmimAc, $\geq$ 95 %, BASF, Ludwigshafen, Germany) was used as the cellulose solvent. Prior to use, the textile and IL were dried under vacuum at 85 °C for at least 24 h and 5 days, respectively, in order to exclude the influence of adsorbed moisture on cellulose dissolution.

2.2. Fabrication of ACC laminates

A laminate stack with 1, 2, 4 or 8 laminae was infused with the IL using a rectilinear setup (Figure 1a) as previously described elsewhere [11]. Briefly, ACC laminates (ca. 180 $\times$ 350 mm^2) were fabricated with a symmetric layup, with laminae aligned such that the warp direction was parallel to the infusion direction. Infusion with BmimAc was carried out at an absolute pressure of 200 mbar. Partial dissolution of the cellulose precursor was carried out in a laboratory hot press (Gibitre Instruments, Bergamo, Italy) at 95 °C under an applied pressure of 1 MPa for 60 min. The application of equal infusion pressure and dissolution time ensured homogeneous solvent uptake and matrix creation by partial dissolution in all laminates. The partially dissolved textiles were then regenerated and washed in distilled water at room temperature (20 $\pm$ 2 °C) with two water changes per day until no further increase in conductivity of the water bath was measured, indicating complete removal of the solvent. For comparison, a single layer laminate required a washing time of 3 days, while that with 8 laminae required 10 days. The removal of BmimAc was confirmed by Fourier-transformed infrared spectroscopy (FTIR). The regenerated material was cut for field emission SEM and tensile testing using a sharp blade. The specimens were then dried between porous polytetrafluoroethylene (PTFE) sheets (2 mm thick, pore size 20 µm, DIA-Nielsen GmbH & Co. KG, Düren, Germany) at 60 °C under vacuum and an external pressure of 0.2 MPa until their mass was constant (Figure 1a).

An unreinforced cellulose film was prepared by dissolving 10 wt.% rayon (fibres of ~2 mm length) in BmimAc at a temperature of 95 °C for 60 min while continuously stirring. The cellulose-BmimAc solution was centrifuged at 3000 rpm for 10 min so as to degas the solution and separate undissolved cellulose residues. Subsequently, the solution was cast into a rectangular mould consisting of a 3 mm thick polypropylene plate with a rectangular opening of 55 mm length and 35 mm width sandwiched between two sheets of porous PTFE. The mould was submerged in distilled water and vacuum was applied so as to infiltrate the porous PTFE with water. The film was left to regenerate over night, removed from the mould and subsequently washed and dried as described above.

Figure 1

2.3. Materials characterisation

The ACC laminates were tensile tested according to ASTM D 3039 on a universal testing machine (Criterion 43, MTS Systems Corporation, Eden Prairie, USA) with a 500 N, 2.5 kN or 10 kN load cell using a minimum of 6 replicates. Non-contact displacement measurement was carried out with a video extensometer (Genie 1400, Teledyne DALSA, Waterloo, Canada). Rectangular specimens with a width of 14 mm and gauge length of 65 mm were tested at a constant crosshead speed of 2 mm min^{-1}. The tensile load was applied parallel to the warp direction (Figure 1b). The unreinforced cellulose film was tested as rectangular specimens with a width and gauge length of 4 mm and 15 mm, respectively. All tensile specimens were conditioned at 23 °C and 50 % RH for a minimum of 24 h prior to testing.

Young's modulus was determined as tangent modulus between strains of 0.1 % and 0.3 %. The work to fracture was determined by numerically integrating the stress-strain curve. Results are given as the arithmetic mean ± standard deviation. The differences in the observed mechanical properties were tested for statistical significance at a probability level of 5 % by analysis of variances using the programming language R [16].

The density of oven-dried ACC laminates was determined by measuring their mass in both air and distilled water using an analytical balance equipped with the corresponding density determination kit (XP 105, accuracy d = 0.01 mg, Mettler Toledo, Greifensee, Switzerland). The volume fraction of voids V_v was calculated according to ASTM-D2734 based on the assumption that the final density of the ACC (ρ_{ACC}) should be equal to that of the dry rayon fibres (ρ_{rayon} = 1.52 g cm^{-3} [22]) if the ACC is void-free and exhibits a constant overall crystallinity ($V_v = \rho_{rayon} - \rho_{ACC}) / \rho_{rayon} \times 100$). The matrix fraction V_m was determined by image analysis of scanning electron micrographs. The low contrast between fibre and matrix in the micrographs required manually delineating the

matrix phase by image manipulation (GIMP 2.8.2, www.gimp.org). The resulting high contrast images were analysed using the threshold tool in ImageJ 1.49g (Wayne Rasband, National Institute of Health, USA). V_m was calculated by dividing the number of matrix pixels by the number of pixels of the full image.

A series of specimens were prepared for WAXD by microtoming 80 µm thick slices from an 8 layer laminate from the surface (skin) through to the core of the laminate. The thin slices were analysed in a x'pert powder diffractometer (PANalytical, Almelo, Netherlands) equipped with a sample spinner. The cobalt anode ($\lambda = 1.790307$ Å) was excited at a voltage of 40 kV and current of 40 mA. Data acquisition was performed in powder mode in steps of 0.1° over a 2θ range of 10° to 40°. Diffractograms were then recalculated for a copper anode ($\lambda = 1.54184$ Å) for easier comparison with the literature. The machine background was subtracted from the diffractograms prior to peak fitting using Pearson VII profiles with Fityk (Version 0.9.8; [17]). Cellulose crystallinity was determined *via* the integral method [18] by integrating the fitted functions from 2θ = 10° to 40° using Matlab (R2014a, MathWorks, Natick, MA, USA) and calculating their ratio. In absence of an amorphous cellulose standard, a background signal was computed from data presented by Duchemin et al. [19].

2.4. Damage evolution

The tensile damage evolution of ACC laminates was examined following the approach proposed by Lomov et al. [20]. Damage analysis began with tensile testing specimens to failure. Characteristic strain levels for a *post-mortem* investigation were then determined from the stress-strain curves. New specimens were then loaded in tension to strains of 0.5 % (ε_1), 1.5 % (ε_2) and 4.5 % (ε_3) after which the specimens were immediately unloaded and the accumulated damage analysed by SEM.

Longitudinal and transverse cross sections of the tensile specimens (Figure 1b) were obtained by cutting 10 mm long blocks from the gauge length region. The blocks were then softened by immersion in distilled water for 1 h so that a smooth surface for SEM analysis could be prepared by cutting with a razor blade. The prepared blocks were dried under the same conditions as the laminate and gold coated for 180 s at 25 mA (Emitech K975X, Quorum Technologies Ltd, East Grinstead, UK). Three replicates per strain level were examined using a field emission scanning electron microscope (7000F FE-SEM, JEOL, Tokyo, Japan) using an accelerating voltage of 5 kV. SEM observations of re-wetted, cut and re-dried ACC laminates showed no influence of the sample preparation procedure on the composite microstructure.

3. Results and discussion

3.1. Microstructure

Dimensionally stable laminates were produced by SIP due to thorough consolidation between and within the laminae. The individual rayon fibres were partially or fully surrounded by a layer of matrix phase approximately 1 to 5 µm in thickness, indicative of partial dissolution of the fibres. A similar matrix content of ca. 7 % was found in all laminates (Table 1). Longitudinal and transverse cross sections revealed identical microstructures with alternating warp and weft yarns according to the weave pattern of the precursor textile (Figure 2). Low numbers of voids (~10 µm diameter) were observed between the laminae and in between fibres. Figure 2

3.2. Tensile properties

The stress-strain curve of ACC laminates with 4 laminae exhibited linear elastic behaviour up to the yield point at 62 to 67 MPa and ca. 1.5 % strain (Figure 3). The yield point was followed by a stress plateau that extended until fracture occurred at a strain of 4.8 ± 2.1 %. The stress-strain curve could be divided into four distinct stages: (I) linear-elastic, (II) yielding, (III) stress plateau after yielding and (IV) final failure (Figure 3). A detailed microstructural characterisation of the accumulated damage in Stages I to IV was carried out at nominal strains of 0.5 % (ε_1), 1.5 % (ε_2), 4.5 % (ε_3) and strain at failure (ε_f). Figure 3

3.3. Damage evolution in all-cellulose composite laminates

The as-processed ACC laminates were semi-transparent, which is typical for ACCs that exhibit thorough consolidation and interfacial adhesion between fibre and matrix [21]. A similar level of translucency was retained in specimens strained to 0.5 % and 1.5 % (Figure 4). Microscopic observations revealed no difference in microstructure between as-processed and 0.5 % strained specimens. No cracks or debonding of fibre and matrix were observed in longitudinal and transverse cross sections in Stage I. The initiation of failure occurred in Stage II upon yielding, resulting in the appearance of microcracks observed in specimens strained to 1.5 % (Figure 6). Microcracks of 2 to 10 µm length were orientated perpendicular to the applied tensile load, and appeared to mainly originate from microvoids (Figure 6). No damage was evident in the transverse cross section.

The observation of larger cracks of 10 to 30 µm width and 100 to 300 µm length propagating through the transverse weft yarns after applying a strain of 4.5 % (Stage III, Figure 7) was concomitant with an increase in the opacity of the specimens. The opacity of the specimen gauge section

increased with strains up to 4.5 % (ε_3); dark lines were also observed to appear at this level of strain (Figure 4). Transverse yarns were split by cracks, while the longitudinal warp yarns remained intact. In this way, the longitudinal warp yarns were observed to function as crack arresters. Furthermore, the regions of matrix phase between weft yarns exhibited cracking. Consequently, the separation of yarns resulted in local delamination of adjacent laminae (Figure 7).

Longitudinal cross sections of fractured specimens (Stage IV) exhibited extensive accumulation of cracks and delamination (Figure 8). The damage was accompanied by a further increase in opacity in the gauge section with increasing strain until fracture (Figure 4). Approximately half of the transverse yarns were split completely, some by two or more cracks (Figure 8). The cracks in transverse yarns propagated in between fibres with some fibres separated from the edge of cracks, and fibre splitting rarely occurred (Figure 9). Local delamination was caused by long cracks originating from the fracture surface and propagating longitudinally in between laminae (Figure 8). Pull-out of complete yarns could be observed at the fracture surface (Figure 10a). However, there was little evidence of individual fibre pull-out (Figure 10b,c).

The increase in opacity with increasing strain was only observed for thick laminates based on 4 and 8 laminae. Laminates based on 1 and 2 laminae were semi-tranparent even after being strained to failure, similar to the appearance of as-fabricated specimens. However, visual observation revealed individual transverse cracks close to the site of fracture (Figure 5).

Figure 4
Figure 5
Figure 6
Figure 7
Figure 8
Figure 9
Figure 10

3.4. *Physical properties and fine structure of all-cellulose composite laminates as a function of laminate thickness*

3.4.1. *Thickness and density*

The thickness of the ACC laminates increased from 0.42 ± 0.04 mm for 1 lamina to 3.36 ± 0.04 mm for 8 laminae (Table 1). Laminate thickness increased by 703.6 %, which was slightly higher than the theoretically expected value of 700 %. Simultaneously, the density of the ACC laminates decreased by 1.3 % from $1.501 \pm 0.002\,\mathrm{g\,cm^{-3}}$ for 1 lamina to $1.481 \pm 0.005\,\mathrm{g\,cm^{-3}}$ for 8 laminae (Table 1). The final density of the ACC (ρ_{ACC}) should be equal to that of the dry rayon fibres (ρ_{rayon} = $1.52\,\mathrm{g\,cm^{-3}}$ [22]) if the ACC is void-free and exhibits a constant overall crystallinity. Hence, the void content ($(\rho_{\mathrm{rayon}} - \rho_{\mathrm{ACC}})/\rho_{\mathrm{rayon}} \times 100$) of a single lamina is 1.3 %, which increases to 2.6 % for an 8 laminae ACC (Table 1).

Table 1

3.4.2. Variation of cellulose crystallinity with ACC laminate thickness

As expected, the WAXD diffractograms of all samples produced diffraction peaks at 2θ of 12.3°, 20° and 22° (Figure 11) that are assigned to the diffracting planes ($1\bar{1}0$), (110) and (020) of cellulose II [23]. It is concluded, that the cellulose II polymorph known for rayon fibres [24] remains unchanged with processing into ACC laminates.

The cellulose crystallinity index of an 8 layer laminate was determined as a function of thickness. It increased from 0.64 at the skin to 0.79 in the core of the laminate (Figure 11). Cellulose is a semicrystalline polymer and its crystallinity is known to change with dissolution and subsequent regeneration [25–27]. The regeneration of cellulose from a solution relies on the counter-diffusion between the non-solvent in the coagulant, in this case water, and the solvent in the cellulose solution [26]. As the water penetrates into the cellulose solution and the IL into the water bath, the intra- and intermolecular hydrogen bonds are reformed and the cellulose precipitates. Jiang et al. have shown that the diffusion of IL from a cellulose solution in water follows Fick's Law, IL diffuses from regions of high concentration to regions of low concentration along a concentration gradient, and the diffusion coefficient depends on temperature, cellulose content in the solution and IL concentration in the regeneration bath [28]. Thin ACC laminates have a high surface to volume ratio such that the IL and water need only diffuse short distances to allow rapid regeneration of the partially dissolved rayon. Thick laminates have a lower surface to volume ratio and an increased length over which IL and water have to diffuse, which results in longer regeneration times. Furthermore, only the skin is directly exposed to the water bath. In accordance with Fick's law, at any given time following regeneration, the relative IL concentrations are higher in thicker laminates. The slower regeneration results in a more crystalline arrangement of cellulose chains [25–27, 29] and hence the crystallinity increases towards the core of thick laminates (Figure 11).

An increase in crystallinity may have an effect on the mechanical properties of ACCs. Hindeleh has shown that the tensile strength and Young's modulus of viscose rayon fibres increases with increasing crystallinity [30]. Similarly, an increase in crystallinity was linked to an increase in tensile strength of regenerated cellulose films [26, 31] and to an increase in Young's modulus and tensile strength of ACCs produced by partial dissolution of microcrystalline cellulose in LiCl/N,N-dimethylacetamide [27]. An increase in Young's modulus of 2.7 % from 7.3 ± 0.4 GPa in 1 lamina to 7.5 ± 0.5 GPa in 8 laminae ACCs was found, although the differences were not found to be significant.

The increase in crystallinity also has an impact on the density of ACC laminates, as amorphous cellulose is 5 to 6 % less dense than crystalline cellulose [32]. The increased crystallinity may be equalled to a change in the ratio of amorphous to crystalline cellulose ($R_{a/c}$). Changes in density are then estimated using the rule of mixtures. Given the density of crystalline and amorphous cellulose II is 1.58 g cm^{-3} [22] and 1.47 g cm^{-3} [33], respectively, a change in $R_{a/c}$ from 0.36/0.64 at the skin to 0.21/0.79 at the core of 8 layer laminates results in a 1.1 % higher density at the core. Averaged over the full thickness of an ACC laminate, this equates to an increase in density of 0.55 % for a laminate with 8 laminae when compared to 1 lamina.

However, the overall change in density of ACC laminates by increasing the number of laminae is negative. The increase in density by approximately 0.5 % due to the higher crystallinity at the core of 8 layer laminates (Figure 11) is counteracted by the laminate thickness increasing by 3.6 % more than the expected 700 % (Table 1). This leads to the observed increase in void content by 1.3 % when comparing laminates based on 1 and 8 laminae.

Figure 11

3.4.3. Variation of mechanical properties with increasing ACC laminate thickness

The ACC laminates were found to exhibit a positive size effect of increasing ultimate tensile strength, yield strength and elongation at break with increasing thickness. The ultimate tensile strength increased from 79.7 ± 1.4 MPa to 105.8 ± 4.2 MPa (+32.8 %) as the number of laminae was increased (Table 1). The shape of the stress-strain curves of ACC laminates also changed with increasing number of laminae (Figure 12). Initially, all of the laminates exhibited linear elastic behaviour prior to yielding between 1 and 2 % strain. No significant change in Young's modulus was found. The yield strength increased from 60.9 ± 0.3 MPa to 66.5 ± 3.3 MPa by increasing the number of laminae from 1 to 8. A more pronounced plateau in stress was observed following yielding of laminates with 4 and 8 laminae. The stress plateau extended from approximately 3 to 9 % strain with 8 laminae. This led to an increase in strain to failure by 187 % from 3.1 ± 1.2 % to 8.9 ± 1.0 % when the number of laminae was increased from 1 to 8.

An unreinforced film of fully dissolved rayon, a representation of the pure matrix phase, exhibited a tensile strength of 66.9 ± 5.3 MPa and Young's modulus of 7.1 ± 0.6 MPa. The film fractured at a comparatively low strain of 2.0 ± 0.9 % (Figure 12 & 13), probably due to the absence of long range cohesion of the fibres present in the ACC laminates. It needs to be noted that the structure and properties of the unreinforced film may differ from the actual matrix phase in the ACC laminates. The crystallinities may be different, as the surface of the partially dissolved fibres may act as nuc-

leation site for the matrix during regeneration and the film is regenerated within a porous mould, whereas the laminates are in direct contact with the washing bath. Consequently, the regeneration rate may be different which could also lead to a different crystallinity. Furthermore, the matrix is approximately 1 to 5 µm thick, while the unreinforced film has a thickness of 0.26 mm, hence tensile testing may also be affected by a size effect. The intricacies of 1-step processing make it virtually impossible to prepare a cellulose film that exactly resembles the matrix phase of ACC laminates. The preparation conditions of the films tested here are as close to those of the matrix as possible, however, due to the differences noted above the comparisons to the actual matrix phase need to be drawn with care.

Figure 12

Figure 13

3.5. Positive size effect on tensile strength of ACC laminates

The increase of mechanical properties with increasing thickness of ACC laminates is surprising, as a size effect of decreasing strength with increasing volume is generally known for composites [13, 14]. The reasons for the increased mechanical properties were found to lie within the structure and damage evolution of ACC laminates, as discussed in the following sections.

3.5.1. Strengthening mechanism in thick ACC laminates

The most prominent difference in the tensile characteristics of thin (1 and 2 laminae) and thick laminates (4 and 8 laminae) is the stress plateau (Stage III) following yield (Figure 12). This plateau coincides with an increase in opacity of the thicker laminates during tensile testing (Figure 4). The opacity of the specimens can be correlated with damage that accumulates during Stage III. Cracking of transverse yarns and delamination are observed, that lead to scattering of light and hence an increase in opacity (Figure 7). The opacity of thick laminates increased during deformation, while the single lamina ACC remained semi-transparent during deformation, indicating a distinct difference in damage accumulation. Furthermore, the longitudinal cross section of fractured thick laminates showed accumulated cracks and local delamination across the entire gauge length. This leads to the conclusion, that thick laminates are more damage tolerant and the following strengthening mechanism is proposed: Transverse cracking and delamination lead to the separation of longitudinal yarns from transverse yarns, which allows the longitudinal yarns to straighten in the direction of the applied load. The straightening allows the yarns to relax from their undulated shape imposed by the weave, thereby reducing tensile stress at a given strain. Thus, the individual yarns remain intact up to higher loads and strains. Furthermore, when a transverse yarn cracks, load is transferred to the

remaining cross sectional area, leading to a local stress concentration. In a single layer such a crack running through a transverse yarn means a loss of 50 % of the cross sectional area that carries load, which equals a stress increase of 100 % (Figure 14). This local jump in stress by 100 % exceeds the strength of the remaining cross section and causes failure of the laminate. Consequently, the first transverse crack that spreads over the full width of a specimen causes a single lamina to fail. In an 8 layer laminate the cracking of a transverse yarn translates to a stress increase of only 6.25 %, the adjacent longitudinal yarns act as crack arresters and the load is transferred to the remaining 7.5 layers (Figure 14). A local increase in stress of 6.25 % does not cause failure and as transverse cracks originate from randomly distributed defects, they occur in the entire gauge volume and the stress redistribution allows the accumulation of many transverse cracks in thick laminates.

In summary, thick laminates have a higher damage tolerance due to crack arresting and stress redistribution. The accumulation of damage within the gauge volume results in the delocalisation of strain, due to the straightening of detached longitudinal yarns. This leads to a transition from early fracture of thin laminates with 1 and 2 laminae at low strains to failure at higher stresses and strains of thick laminates with 4 and 8 laminae.

Figure 14

3.6. *Size effects in composites and polymers*

In the field of composites, the vast majority of studies covers *negative* size effects of decreasing strength with increasing volume [13, 14, 34]. Sutherland et al. [15] mention the existence of a *positive* or reverse size effect of increasing strength with increasing dimensions in composites in their review, although no citations to respective studies are provided. Evidence for the existence of a negative size effect in composites is summarised by Zweben [12] and there are many studies that present experimental evidence [13, 14, 35].

Bazant et al. have shown that Bazant's size effect law applies to composites, according to which the logarithm of strength over the logarithm of specimen size transitions smoothly from a horizontal asymptote predicted by the strength criterion of plastic limit analysis to an inclined asymptote with a slope of -0.5 predicted by linear elastic fracture mechanics [13]. However, their study investigated two-dimensional scaling (primarily width) at constant thickness and is hence not adequate for comparison to the thickness dependent size effect presented in this work.

In general, the negative size effect in composites is attributed to the higher probability of a larger volume to contain a critical defect and it can be modelled by applying Weibull theory to anisotropic materials (modified weakest link model) [14, 36]. The size effect of quasibrittle composites following

the modified weakest link model is characterised by a negative slope in a log-log plot of strength as a function of specimen dimension (Figure 15), which fits experimental data for carbon and glass fibre reinforced composites [14]. On the contrary, ACC laminates of increasing thickness show a positive slope (Figure 15). It needs to be noted, that the application of Weibull theory to size effects in composites has to be treated with care. As Wisnom [14] and Sutherland et al. [15] point out in their reviews, Weibull theory assumes that failure occurs catastrophically from a critical defect. Failure of carbon and glass fibre-reinforced composites often occurs suddenly, initiating from a defect and resulting in brittle failure, hence Weibull can be applied [14, 15]. In contrast, the failure of ACC laminates is characterised by extensive damage accumulation, which distinguishes them from composites characterised by a Weibull-type size effect.

Figure 15

A fundamental difference between conventional composites and ACCs is that in carbon and glass fibre-reinforced composites brittle fibres are embedded in a more ductile matrix and the overall properties resemble a quasibrittle material, whereas in ACC laminates ductile fibres are joined by a matrix that fails at lower strains. The damage evolution in composites based on woven textile precursors of glass and carbon fibre is similar to that described for ACC laminates, with damage initiating in transverse yarns and subsequent damage accumulation in the form of cracks and delamination. However, in glass and carbon fibre-reinforced composites damage initiation causes a less pronounced decrease in stiffness and damage accumulation only occurs over a narrow strain region before laminate failure occurs [37–40]. In contrast, a stress plateau after yield that extends to high strains of up to 10 % was observed in thick ACC laminates. The reasons for this particular behaviour are thought to lie in the ductility and high toughness of the rayon fibres used as precursor [55], which allows extensive damage accumulation and results in the increased tensile strength of thick laminates.

The potential of thick ACC laminates to accumulate damage shows that the existence of defects in these new materials is not detrimental to strength, but is instead part of the strengthening mechanism described above. A higher void content has been shown to lead to a decrease in strength of carbon-epoxy [41] and flax-epoxy composites [42]. In ACC laminates, on the contrary, the increase in void content with increasing laminate thickness (Table 1) could be beneficial to the strengthening mechanism by initiating transverse cracks (Figure 6). However, an increase in void content also leads to a decrease in interfacial shear strength of 7 % per 1 % voids [43]. The relative contribution of

increased void content and reduced interfacial shear strength to the initiation and accumulation of damage is not evident from the present work and will be addressed in more detail in future studies.

While a negative size effect is known for a variety of materials, e.g. concrete, rock, ceramics and wood [44] as well as metals such as aluminium [45], a positive size effect as seen in ACC laminates is rare. Exceptions from the generally negative size effect have been reported for concrete in splitting tensile tests, depending on the loading configuration [46, 47], for sea ice under certain conditions [48] and depending on thickness and orientation in hot extruded magnesium alloy [49].

Polymers and polymer fibres are also subject to a negative size effect caused by the higher number of flaws and their increasing size with increasing specimen volume [50, 51]. The toughness of brittle polymers can be increased by several mechanisms as outlined by Argon and Cohen [52]. While an increase in microstructural perfection to avoid critical flaws by optimising polymer processing is either fundamentally not possible or costly, a transition to ductile failure in semi-crystalline polymers can be achieved by lowering the plastic resistance. An effective way of enhancing plasticity is the quasi-uniform cavitation of a polymer by the introduction of particles. Upon the application of stress, the particles cause cavitation or debond and the polymer undergoes large scale strain in the interparticle ligaments, leading to global delocalisation of strain and a transition to ductile behaviour [52].

The same toughening concept applies to ACC laminates. The transverse cracking of weft yarns leads to their debonding from the longitudinal yarns. The straightening of longitudinal yarns from their undulation in the weave pattern in turn results in an increase in strain. As transverse cracking is a global phenomenon occurring in the entire gauge volume of thick laminates, it results in global strain delocalisation and an overall transition to ductile behaviour of thick ACC laminates. In addition to strain delocalisation, crack deflection at the point where transverse cracks meet longitudinal yarns and interlaminar debonding (Figure 7) are known as efficient energy absorbers in composites [53] that contribute to the increase in toughness with increasing ACC laminate thickness, with the work to fracture of 1.3 ± 0.4 MJ m^{-3} in 1 lamina increasing to 8.2 ± 1.1 MJ m^{-3} in 8 laminae ACCs.

3.7. *Initiation of failure in ACC laminates*

The yielding of ACC laminates occurs at 1 to 2 % strain, which is similar to rayon fibres [54, 55]. The typical double-linear increase in stress with strain of regenerated cellulose fibres is due to a linear change in orientation of crystalline and amorphous domains with the disruption of interfibrillar hydrogen bonds at yield leading to a decrease in slope at higher strains [56, 57]. However,

the change in slope after yield is less pronounced in rayon fibres than in ACC laminates; stress still increases from ca. 300 MPa to ca. 800 MPa after the yield of fibres [55], while the increase in stress plateaus with yield in ACC laminates (Figure 12). It is therefore concluded that the onset of microstructural damage in ACC laminates coincides with the yield point, confirmed by the first occurrence of microcracks in transverse yarns in Stage II (Figure 6).

Damage is expected to initiate either from the fibres, the matrix or from the interface. Splitting of fibres was only observed once and can be ruled out (Figure 9c). The matrix is observed to separate from fibres in microcracks (Figure 9a) and the unreinforced cellulose film broke at stress and strain levels similar to the yield strength of laminates (Figures 12 & 13), suggesting that the matrix strength is reached with yield. The interfacial strength of a cellulose fibre bonded to a matrix of regenerated cellulose is not known, although, the fracture surface of ACC laminates showed no fibre pull-out (Figure 10), an indicator of good interfacial bonding [53]. Unfortunately, the low contrast between fibre and matrix in SEM micrographs impedes a clear distinction of interfacial and matrix failure.

In summary, the fracture surface of ACCs, which indicates strong interfacial bonding, and the similarity of unreinforced film strength and laminate yield strength suggest that damage initiation by matrix failure is more likely than interfacial failure, however, the low contrast in SEM micrographs does not allow a definite conclusion.

3.8. Scale effect

Sutherland et al. point out that a scale effect (difference in manufacturing quality between small samples and large structures) can dominate over a size effect, as shown for glass fibre reinforced composites [58]. All samples in this study were processed using the same equipment and great care was taken to prevent a scale effect. However, two aspects of the positive size effect in ACC laminates, the increase in void content and crystallinity, are affected by scaling. The increase of laminate thickness by adding layers increases the likelihood of air inclusions during SIP, hence the higher void content of thicker laminates can be considered a scale effect. The regeneration of dissolved cellulose is affected by scale, due to the decelerated diffusion with increased thickness, as discussed above. The higher crystallinity at the core of thick laminates can therefore also be considered the result of a scale effect.

4. Conclusions

This work demonstrates that the solvent infusion process allows the upscaled manufacture of ACC laminates without compromising their mechanical properties. Increasing the thickness of solvent infusion processed ACC laminates based on a woven cellulose textile leads to a transition from failure of thin laminates (1 and 2 laminae) at comparatively low strains and stresses to a tough and ductile behaviour of thick laminates (4 and 8 laminae) with failure at higher stress and strain levels. The changes in mechanical properties with increasing laminate thickness are due to a combination of scale and size effects. The positive size effect of increasing ultimate tensile strength and work to fracture is attributed to a higher damage tolerance of thick laminates. Stress redistribution upon cracking of transverse yarns allows damage accumulation in thick laminates, which results in global strain delocalisation, increased ductility and higher ultimate tensile strength. Increasing laminate thickness by the addition of layers leads to a higher void content in thick laminates. This scale effect contributes to the strengthening mechanism, as transverse cracking initiates from voids. A further scale effect is the increase in cellulose crystallinity at the core of thick laminates due to decelerated regeneration.

Acknowledgements

The authors acknowledge the financial support of the Dumont d'Urville New Zealand-France Science & Technology Support Programme. The authors are grateful to Cordenka GmbH & Co. KG (Obernburg, Germany) and Mr R. Einsiedel for kindly providing the rayon textiles. The authors thank Mr M. Flaws and Mr K. Stobbs for technical assistance. J. Dormanns thanks the University of Canterbury for granting a UC Doctoral scholarship.

References

References

[1] Bledzki AK, Gassan J. Composites reinforced with cellulose based fibres. Prog Pol Sci 1999; 24(2):221–274.

[2] John M, Thomas S. Biofibres and biocomposites. Carbohydr Pol 2008;71(3):343–364.

[3] Faruk O, Bledzki AK, Fink HP, Sain M. Biocomposites Reinforced with Natural Fibers: 2000-2010. Prog Pol Sci 2012;37(11):1552–1596.

[4] Nishino T, Matsuda I, Hirao K. All-cellulose composite. Macromolecules 2004;37(20):7683–7687.

[5] Matabola KP, De Vries AR, Moolman FS, Luyt AS. Single polymer composites: a review. J Mater Sci 2009;44(23):6213–6222.

[6] Karger-Kocsis J, Bárány T. Single-polymer composites (SPCs): Status and future trends. Compos Sci Tech 2014;92:77–94.

[7] Huber T, Müssig J, Curnow O, Pang S, Bickerton S, Staiger MP. A critical review of all-cellulose composites. J Mater Sci 2012;47(3):1171–1186.

[8] Kalka S, Huber T, Steinberg J, Baronian K, Müssig J, Staiger MP. Biodegradability of all-cellulose composite laminates. Composites Part A 2014;59:37–44.

[9] Gindl W, Keckes J. All-cellulose nanocomposite. Polymer 2005;46(23):10221–10225.

[10] Huber T, Pang S, Staiger MP. All-cellulose composite laminates. Composites Part A 2012; 43(10):1738–1745.

[11] Huber T, Bickerton S, Müssig J, Pang S, Staiger MP. Solvent infusion processing of all-cellulose composite materials. Carbohydr Pol 2012;90(1):730–733.

[12] Zweben C. Is there a size effect in composites? Composites 1994;25(6):451–454.

[13] Bažant Z, Daniel I, Li Z. Size effect and fracture characteristics of composite laminates. J Eng Mat Tech 1996;118(3):317–324.

[14] Wisnom M. Size effects in the testing of fibre-composite materials. Compos Sci Tech 1999; 59:1937–1957.

[15] Sutherland L, Shenoi R, Lewis S. Size and scale effects in composites: I. Literature review. Compos Sci Tech 1999;59:209–220.

[16] R Core Team. R: A Language and Environment for Statistical Computing. R Foundation for Statistical Computing, Vienna, Austria ISBN 3-900051-07-0, URL http://wwwR-projectorg/ 2013; .

[17] Wojdyr M. Fityk: a general-purpose peak fitting program. J Appl Cryst 2010;43(5):1126–1128.

[18] Wakelin JH, Virgin HS, Crystal E. Development and Comparison of Two X-Ray Methods for Determining the Crystallinity of Cotton Cellulose. J Appl Phys 1959;30(11):1654.

[19] Duchemin B, Thuault A, Vicente A. Ultrastructure of cellulose crystallites in flax textile fibres. Cellulose 2012;19(6):1837–1854.

[20] Lomov S, Ivanov D, Truong T, Verpoest I, Baudry F, Vanden Bosche K, Xie H. Experimental methodology of study of damage initiation and development in textile composites in uniaxial tensile test. Compos Sci Tech 2008;68(12):2340–2349.

[21] Soykeabkaew N, Arimoto N, Nishino T, Peijs T. All-cellulose composites by surface selective dissolution of aligned ligno-cellulosic fibres. Compos Sci Tech 2008;68(10-11):2201–2207.

[22] Woodings C. Regenerated Cellulose Fibres. Cambridge: Woodhead Publishing Ltd, 2001.

[23] French A. Idealized powder diffraction patterns for cellulose polymorphs. Cellulose 2014; 21:885–896.

[24] Röder T, Moosbauer J, Kliba G, Schlader S, Zuckerstatter G, Sixta H. Comparative characterisation of man-made regenerated cellulose fibres. Lenz Ber 2009;87:98–105.

[25] Bang YH, Lee S, Park JB, Cho HH. Effect of coagulation conditions on fine structure of regenerated cellulosic films made from cellulose/N-methylmorpholine-N-oxide/H2O systems. J Appl Pol Sci 1999;73(13):2681–2690.

[26] Zhang L, Mao Y, Zhou J, Cai J. Effects of Coagulation Conditions on the Properties of Regenerated Cellulose Films Prepared in NaOH/Urea Aqueous Solution. Ind & Eng Chem Res 2005; 44(3):522–529.

[27] Duchemin BJC, Newman RH, Staiger MP. Structure-property relationship of all-cellulose composites. Compos Sci Tech 2009;69(7):1225–1230.

[28] Jiang G, Huang W, Zhu T, Zhang C, Kumi AK, Zhang Y, Wang H, Hu L. Diffusion dynamics of 1-Butyl-3-methylimidazolium chloride from cellulose filament during coagulation process. Cellulose 2011;18(4):921–928.

[29] Song H, Niu Y, Yu J, Zhang J, Wang Z, He J. Preparation and morphology of different types of cellulose spherulites from concentrated cellulose ionic liquid solutions. Soft Matter 2013; 9:3013–3020.

[30] Hindeleh AM. X-Ray Characterization of Viscose Rayon and the Significance of Crystallinity on Tensile Properties. Text Res J 1980;50:581–589.

[31] Zhang L, Ruan D, Zhou J. Structure and Properties of Regenerated Cellulose Films Prepared from Cotton Linters in NaOH/Urea Aqueous Solution. Ind & Eng Chem Res 2001;40(25):5923–5928.

[32] Hermans PH, Hermans JJ, Vermaas D. Density of Cellulose Fibers. III. Density and Refractivity of Natural Fibers and Rayon. J Pol Sci 1946;1(3):162–171.

[33] Ishikawa A, Okano T, Sugiyama J. Fine structure and tensile properties of ramie fibres in the crystalline form of cellulose I, II, IIII and IVI. Polymer 1997;38(2):463–468.

[34] Bažant Z, Kim J, Daniel I, Becq-Giraudon E, Zi G. Size effect on compression strength of fiber composites failing by kink band propagation. Int J Fract 1999;95:103–141.

[35] Gurvich M, Pipes R. Strength size effect of laminated composites. Compos Sci Tech 1995; 55:93–105.

[36] Tabiei A, Sun J. Analytical simulation of strength size effect in composite materials. Composites Part B 2000;31:133–139.

[37] Coman F, John S, Herszberg I. Damage progression analysis in 3-D woven composite components. ICCM 12 Conference Paris 1999;Paper 793:1–10.

[38] Zako M, Uetsuji Y, Kurashiki T. Finite element analysis of damaged woven fabric composite materials. Compos Sci Tech 2003;63(3-4):507–516.

[39] Lisle T, Bouvet C, Pastor M, Margueres P, Prieto Corral R. Damage analysis and fracture toughness evaluation in a thin woven composite laminate under static tension using infrared thermography. Composites Part A 2013;53:75–87.

[40] Karahan M. Investigation of damage initiation and propagation in 2 x 2 twill woven carbon/epoxy multi-layer composites. Text Res J 2011;81(4):412–428.

[41] Almeida S, Neto Z. Effect of void content on the strength of composite laminates. Compos Struct 1994;28(2):139–148.

[42] Li Y, Li Q, Ma H. The voids formation mechanisms and their effects on the mechanical properties of flax fiber reinforced epoxy composites. Composites Part A 2015;72:40–48.

[43] Judd CW, Wright W. Voids and their effects on the mechanical properties of composites - an appraisal. SAMPE J 1978;14:10–14.

[44] Bažant ZP, Chen EP. Scaling of Structural Failure. Appl Mech Rev 1997;50(10):593–627.

[45] Bažant ZP, Lee SG, Pfeiffer Pa. Size effect tests and fracture characteristics of aluminum. Eng Fract Mech 1987;26(1):45–57.

[46] Zhou F, Balendran R, Jeary A. Size effect on flexural, splitting tensile, and torsional strengths of high-strength concrete. Cem Conc Res 1998;28(12):1725–1736.

[47] Tang T, Shah SP, Ouyang C. Fracture Mechanics and Size Effect of Concrete in Tension. J Struct Eng 1992;118(11):3169–3185.

[48] Bažant ZP, Guo Z. Size Effect on Strength of Floating Sea Ice under Vertical Line Load. J Eng Mech 2002;128(3):254–263.

[49] Zhang XP, Feng SF, Hong XT, Liu JQ. Orientation-related specimen thickness effects on mechanical properties of hot extruded AZ31B magnesium alloy. Mater Design 2013;46:256–263.

[50] Wagner HD. Stochastic concepts in the study of size effects in the mechanical strength of highly oriented polymeric materials. J Pol Sci Part B 1989;27:115–149.

[51] Odom EM, Adams DF. Specimen size effect during tensile testing of an unreinforced polymer. J Mater Sci 1992;27:1767–1771.

[52] Argon AS, Cohen RE. Toughenability of polymers. Polymer 2003;44(19):6013–6032.

[53] Hull D, Clyne T. An Introduction to Composite Materials. 2nd edition. Cambridge, UK: Cambridge University Press, 1996.

[54] Eichhorn SJ, Young RJ, Yeh WY. Deformation Processes in Regenerated Cellulose Fibers. Text Res J 2001;71(2):121–129.

[55] Adusumali R, Reifferscheid M, Weber H, Roeder T, Sixta H. Mechanical properties of regenerated cellulose fibres for composites. Macromol Symp 2006;244(1):119–125.

[56] Gindl W, Reifferscheid M, Martinschitz KJ, Boesecke P, Keckes J. Reorientation of crystalline and noncrystalline regions in regenerated cellulose fibers and films tested in uniaxial tension. J Pol Sci Part B 2008;46(3):297–304.

[57] Northolt MG, Vries HD. Tensile Deformation of Regenerated and Native Cellulose Fibres. Angew Makromolek Chem 1985;133(2148):183–203.

[58] Sutherland L, Shenoi R, Lewis S. Size and scale effects in composites: III. Woven-roving laminates. Compos Sci Tech 1999;59:235–251.

Tables

Table 1: Mechanical and physical properties of ACC laminates and unreinforced cellulose film (Unr. cell. film). (* significant differences in ultimate tensile and yield strength are indicated by different superscript letters, no significant difference in Young's modulus was found, $p<0.05$.)

	Tensile* strength in MPa	Yield* strength in MPa	Young's* modulus in GPa	Elongation at break in %	Thickness in mm	Density in g cm^{-3}	void content in %	matrix content in %
Unr. cell. film	66.9 ± 5.3^{a}	56.5 ± 6.4^{a}	7.1 ± 0.6	2.0 ± 0.9	0.26 ± 0.10			
1 lamina	79.7 ± 2.4^{b}	60.9 ± 0.3	7.3 ± 0.4	3.1 ± 1.2	0.42 ± 0.04	1.501 ± 0.002	1.3	6.8 ± 0.7
2 laminae	86.0 ± 6.5^{c}	62.4 ± 3.7	7.6 ± 0.3	1.9 ± 0.2	0.88 ± 0.04	1.463 ± 0.019	3.7	7.0 ± 0.5
4 laminae	96.3 ± 3.3^{d}	64.9 ± 2.6^{b}	7.8 ± 0.9	4.8 ± 2.1	1.55 ± 0.05	1.477 ± 0.007	2.8	6.6 ± 0.8
8 laminae	105.8 ± 4.2^{e}	66.5 ± 3.3^{b}	7.5 ± 0.5	8.9 ± 1.0	3.36 ± 0.04	1.481 ± 0.005	2.6	7.3 ± 0.5
change from 1 to 8 laminae	+32.8 %	9.2 %	+2.7 %	+187.1 %	+703.6 %	-1.3 %	+1.3 %	

Figure Captions

Figure 1. Schematic of (a) solvent infusion processing of ACC laminates, and (b) the warp and weft directions in a laminate. The longitudinal and transverse planes describe the cross sections observed in microstructural analysis. Arrows indicate the direction of the tensile load (F) applied during testing.

Figure 2. Scanning electron micrographs of the longitudinal cross section of an as-fabricated 4 layer laminate at varying magnifications.

Figure 3. Representative stress-strain curve of an ACC laminate with 4 laminae characterised by four stages: linear-elastic (I), yield (II), stress plateau (III) and final failure (IV). The accumulated damage was examined at ε_1, ε_2, ε_3 and ε_f.

Figure 4. Photograph of ACC laminates (4 laminae, 14 mm wide) showing increasing opacity with increasing strain. The white star indicates the boundary between the gauge length (opaque) and gripped section (lighter, at bottom) of a fractured specimen, where the gripped section remained mostly unstrained.

Figure 5. Photographs of (a) an as-fabricated and (b) a fractured single lamina specimen (14 mm wide). Arrows indicate the location of individual transverse cracks.

Figure 6. Scanning electron micrographs of the longitudinal cross section of an ACC (4 laminae) strained to 1.5 % elongation (Stage II). Arrow ($\updownarrow$) indicates the direction of the applied tensile stress σ_t.

Figure 7. Scanning electron micrograph of the longitudinal and transverse cross section of an ACC (4 laminae) strained to 4.5 % elongation (Stage III). Direction of the applied tensile stress σ_t is indicated by arrows ($\updownarrow$) for in plane and symbols ($\odot$ & $\oplus$) for out of plane stress.

Figure 8. Scanning electron micrograph of a fractured ACC laminate (4 laminae, Stage IV). Direction of the applied tensile stress σ_t is indicated by arrows ($\updownarrow$).

Figure 9. Scanning electron micrographs of details in split transverse yarns of ACC laminates in Stages III and IV (longitudinal cross section). (a) Transverse crack running in between fibres. (b) Individual fibre separated from other fibres in a yarn and protruding into a transverse crack. (c) Micrograph of the only observed instance of a fibre split by a transverse cracks. The arrow indicates the separated halves of the split fibre.

Figure 10. Scanning electron micrographs of the fracture surface of ACC laminates on (a) laminate, (b) yarn and (c) fibre level.

Figure 11. (a) Normalised XRD diffractograms (shifted vertically for clarity) and (b) cellulose crystallinity as function of thickness of an 8 laminae ACC from skin to core.

Figure 12. Representative stress-strain curves of ACC laminates with increasing number of laminae and unreinforced cellulose film. Graphs have been shifted horizontally for clarity.

Figure 13. Scanning electron micrographs of the fracture surface of the unreinforced cellulose film at low (a) and high (b) magnification.

Figure 14. (a) SEM micrograph with false-coloured inlay showing longitudinal warp (green) and transverse weft yarns (orange). (b) Schematic of the warp and weft yarns of the twill weave textile within the ACC laminates. (c) Schematic of ACCs with 1 lamina and 8 laminae with one fractured transverse yarn and the corresponding increase in stress in the remaining cross-sectional area. (For reference to colours the reader is referred to the web version of the article.)

Figure 15. Log-log plot of tensile strength over specimen volume with a positive slope seen for ACC laminates and a typical negative slope for other composites following Weibull theory [14, 15].

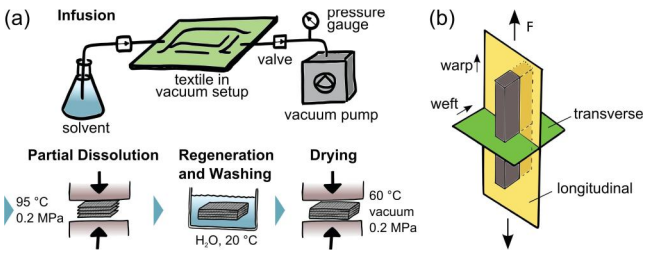

Figure 1

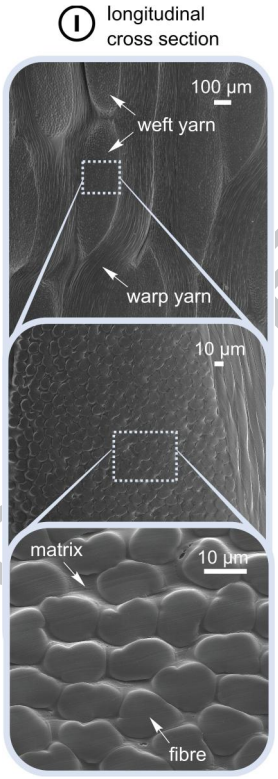

Figure 2

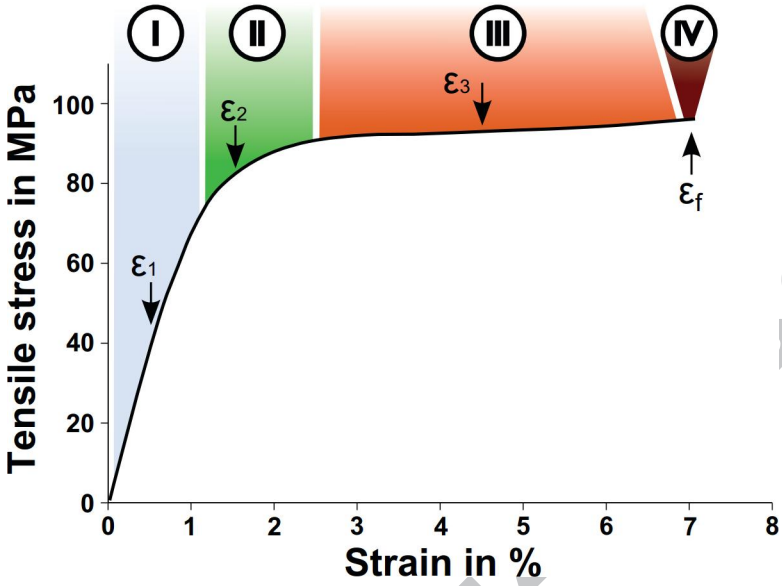

Figure 3

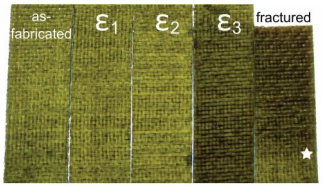

Figure 4

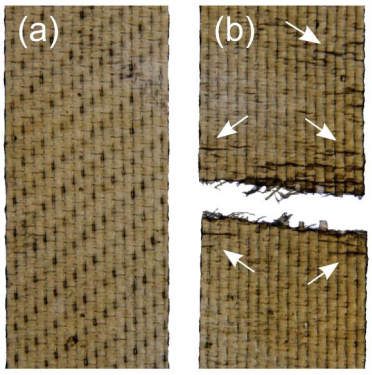

Figure 5

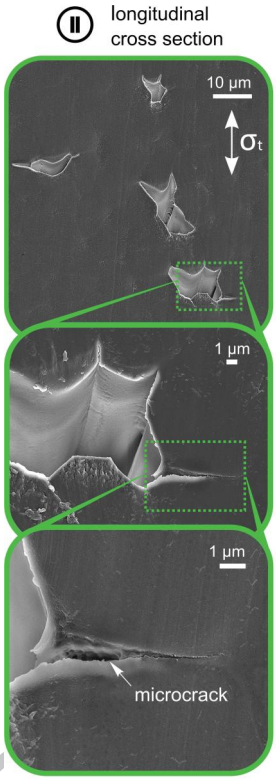

Figure 6

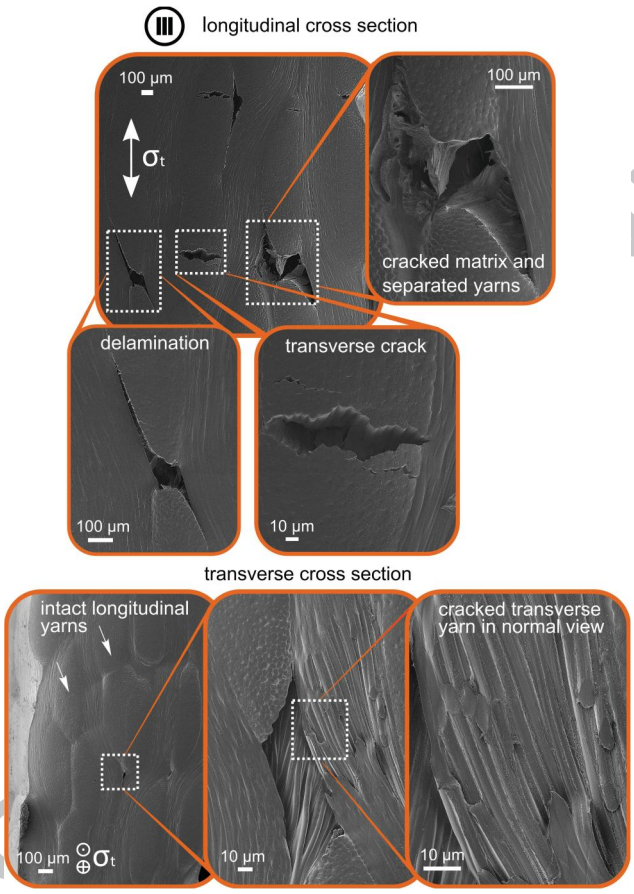

Figure 7

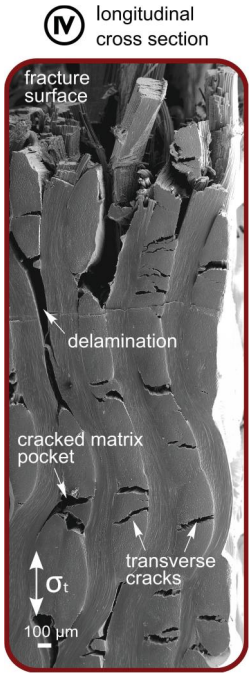

Figure 8

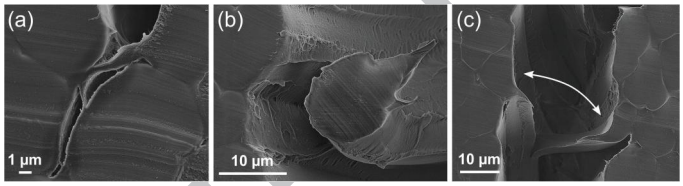

Figure 9

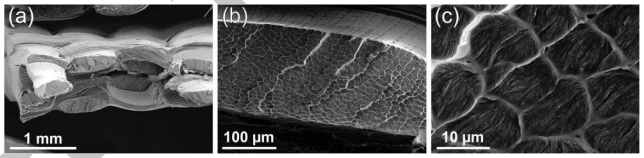

Figure 10

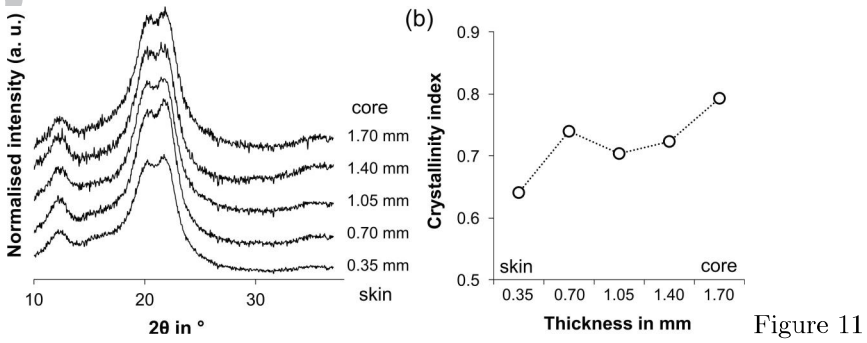

Figure 11

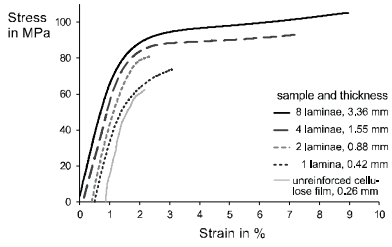

Figure 12

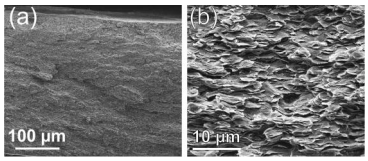

Figure 13

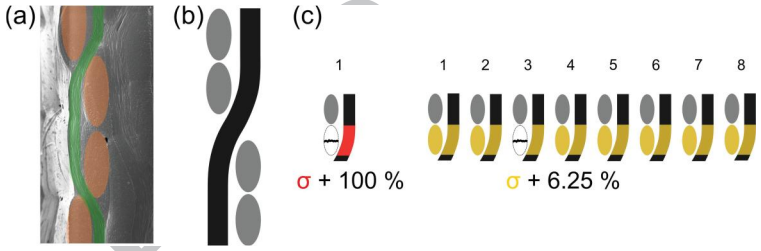

Figure 14

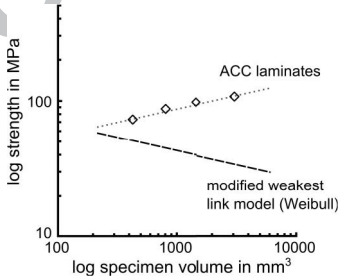

Figure 15